IJUS

International Journal of Unconventional Science
issue 19-20(6), pages 78-97, 2018

received: 09.02.2018
accepted: 23.04.2018
http://www.unconv-science.org/n19/kernbach2
DOI: https://doi.org/10.17613/sp8t-gz69

Biophysical effects of the circular Poynting vector emitter

Serge Kernbach*

***Abstract*—This paper explores biophysical effects of Poynting vector generators that use a circular electromagnetic energy flow in static E/H fields. These devices with circular or cylindrical emitters are popular in the research community as well as among hobbyists in studying influences of weak environmental stimuli on biological and electrochemical systems. Performed tests with liquids based on electrochemical impedance spectroscopy and microbiological samples based on fermentation activity of yeast *Saccharomyces cerevisiae* confirm biophysical effects of such electromagnetic systems. It is demonstrated that effects vary with the axial or radial positions of samples. Several atypical phenomena related to delayed electrochemical dynamics, mismatch with temperature curves, the appearance of 'paradoxical phases' and accumulation of the effect are shown. Developed devices are described in detail for further development as actuators in robotic systems, environmental and biophysical research or other applications.**

I. Introduction

Electromagnetic generators based on a Poynting vector in static E/H fields with circular or cylindrical emitters are popular in various designs. The working principle of such generators consists in creating an orthogonal system of electric and magnetic fields. More formally, the Poynting vector **S** is the vector of energy flux density of the electromagnetic field, which can be defined by the vector product of two vectors:

$$\mathbf{S} = [\mathbf{E} \times \mathbf{H}], \tag{1}$$

where **E** and **H** are vectors of electric and magnetic field. Modern textbooks consider the case of Poynting vector in a cylindrical capacitor, which is located in the H-field created by a permanent magnet, see Fig. 1(a). Although only static electric and magnetic fields exist, the calculation of the Poynting vector gives a circular flow of electromagnetic energy clockwise, see Fig. 1(b). The flow of circulating energy underlies the popular idea of 'rotation' of the **S** vector, which is located in the axial plane in Fig. 1(a) (the circulating energy flow contains the angular momentum and creates the magnetic component of the Lorentz force arising when the capacitor is discharged).

The most common design of these generators includes a disk (ring) magnet and a cylindrical capacitor, see Fig.1(a). Such well-known devices as 'small Akimov's generator' (SAG), see Fig. 2(a), or 'large Akimov's generator' (LAG), see Fig. 2(b), are examples of these generators. Instead of a permanent magnet, electromagnets are often used. A constant voltage is applied to the cylindrical capacitor, in SAG/LAG it varies about 100-200V. Some publications relate them to the so-called 'Tamm's emitters', in following we will denote all emitters of this type as the 'Poynting vector' emitters.

The first design of SAG/LAG dates to the 90s, at the moment there are several descriptions of their design [1], prepared, among others, by E.A.Akimov [2]. Organizations conducting research on 'new physical fields' in the 90s [3] received generators of this type, mainly SAG, for experiments, see Fig. 2(a). The large number of experimental results in the fields of biophysics, metallurgy, see Fig. 2(c), physical chemistry, early spintronics and spin-based signal-transmission were obtained for generators based on the Poynting vector. To some extent, the SAG represents one of the most successful devices of this kind with a great number of publications [4].

There are several descriptions and assumptions about their underlying mechanisms [2], [5]. One of them is devoted to the magnetic vector potential [6], [7], [8]. Open research question, which can serve for explanation of arising effects, is the relationship between the circulating Poynting vector and the Aharonov-Bohm effects [9] and their biophysical manifestations [10], [11]. Another possible explanation goes towards quantum entanglement

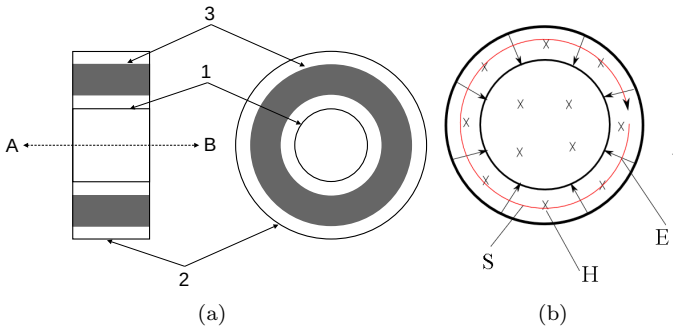

Fig. 1. **(a)** Structure of the SAG/LAG emitters: 1 – inner layer of a cylindrical capacitor, 2 – external layer of a cylindrical capacitor, 3 – ring magnet (or electromagnet). Emission is directed in the axial direction A-B; **(b)** Illustration of the circulating Poynting vector S in static E/H fields, image from Wikipedia.

*CYBRES GmbH, Research Center of Advanced Robotics and Environmental Science, Stuttgart, Germany. This is translated and revised version of the original paper appeared in IJUS, 19-20(6), pp. 78-97, 2018.

(a)

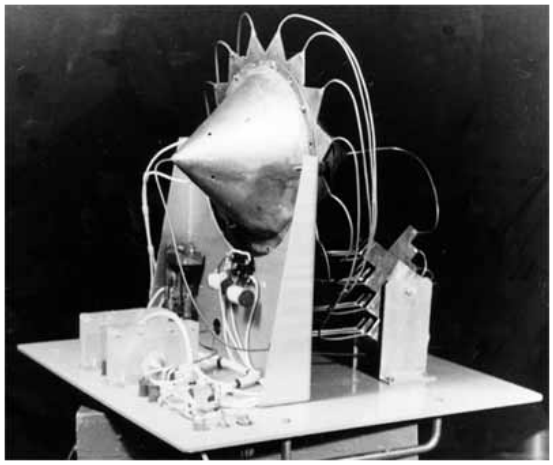

(b)

(c)

Fig. 2. **(a)** One of the SAG constructions used in 80s and 90s; **(b)** Structure of LAG, usage of different geometric elements and metal wires, image from alt-sci.ru; **(c)** Experimental setup based on SAG and used for exposure of solid materials, 2000, Seoul, South Korea, photo courtesy of A.Y.Smirnov.

effects in macroscopic systems [12], [13] with physical [14], [15] and biological [16], [17] phenomena. This idea also pursues the research of external feedback mechanisms, for example, the 'Maslobrod effect' [18], the Smirnov emitters with feedback loops [19], see Fig. 3(a), and other similar developments.

New designs of emitting elements have been appeared in the last years, they deviate from the SAG/LAG 'standard' attempting to create new versions of these devices [20]. For instance, the Fig. 3(b) demonstrates a Planar Poynting vector (PPV) construction with two Helmholtz coils and a flat capacitor. This design allows minimizing the parasitic capacitance between electrodes and the coil. However, tests also showed some disadvantages of PPV emitters, e.g. a missing 'rotation' component.

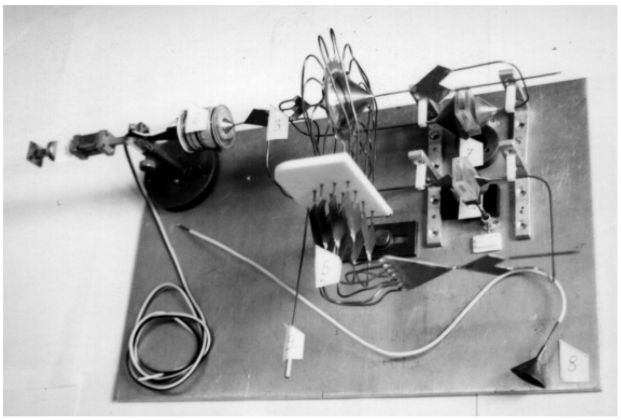

(a)

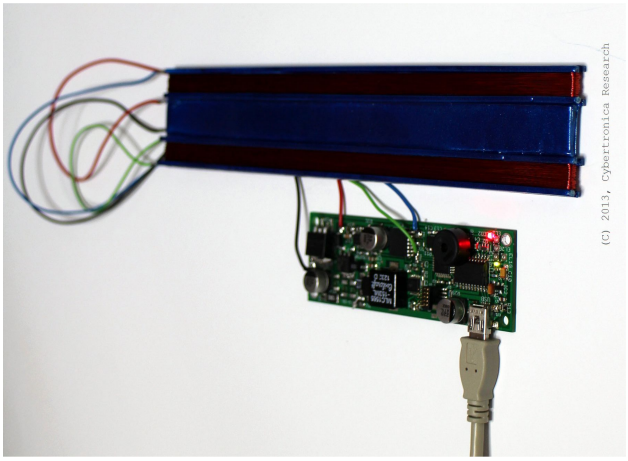

(b)

Fig. 3. **(a)** The Smirnov emitter with feedback loops, image from [19]; **(b)** The Planar Poynting vector (PPV) emitter.

This work returns back to the idea of circulating flow shown in Fig. 1(b). Due to technological reasons, it is advantageous to produce a flat emitter, e.g. as printed circuit boards. Such flat circular emitter generates the rotating Poynting vector 'outside' the emitter (not inside the cylindrical capacitor). In following sections we demonstrate the structure of such Circular Pointing Vector generator (CPV), electronic system, and explore biological (with fermentation activity of yeast *Saccharomyces cerevisiae*) and electrochemical (with electrochemical impedance spectroscopy) effects.

II. Development of the emitter and control electronics

The development of both the emitter and the control module was motivated by ecological and environmental research, e.g. non-chemical treatments of fluids to reduce the amount of chemistry in water [21], [22], [23], exploration of the phase-transition-treatment (PTT) effect

appearing in non-stationary EM fields [24], and several other applications. Especial requirements represent the production technology, i.e. the device must not have parts requiring manual work, such as the wound coils. It makes

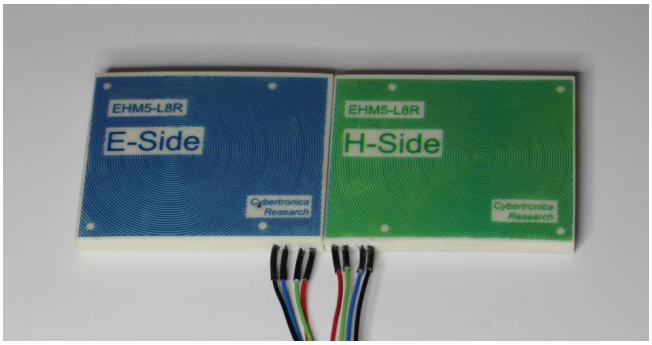

(a)

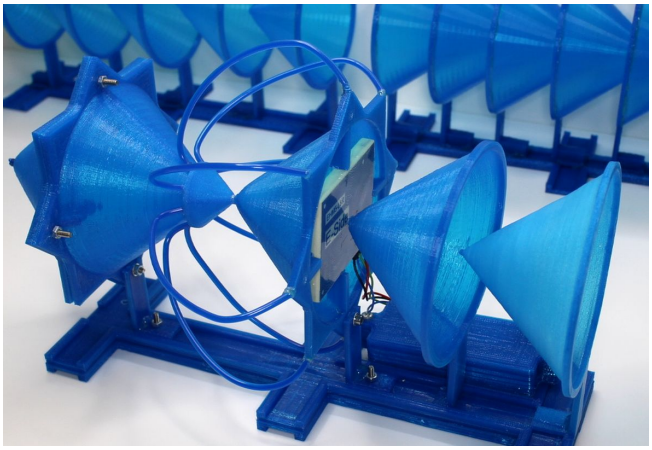

(b)

Fig. 4. **(a)** Multilayer circular Poynting vector (CPV) emitters in a monolithic body; **(b)** Generator based on the shape effect (in the LAG manner) using a monolithic CPV emitter in 2013 [20].

sense to develop not one single-block device, but a kit, where the user can configure the system. The control electronics schould be powered by a USB port or the 'Power bank' accumulators with 5V supply voltage.

Multilayer flat circular emitters have already been developed in research projects, where the multilayer Poynting vector emitters were produced in a monolithic casing, see Fig. 4. These emitters were also used in test generators based on the shape effect early 2013 [20]. However, at that time, the development was concentrated on the Bobrov's LED emitters [25] and the CPV concept was not further followed. The advantage of a flat emitter is its high technological processability, since it can be mass-produced by the technology of printed circuit boards, see Fig. 5(a). It repeats the structure of the E/H fields in Fig. 1(b), but the cylindrical capacitor is replaced by the flat capacitor, and the permanent magnet is replaced by the double flat coil, i.e. the emission element represents a kind of 'circular dipole'. The number of circular dipoles can be increased, see Fig. 5(d), which will scale up the effect. A rotating Poynting vector **S** is generated in the outer part of the emitter.

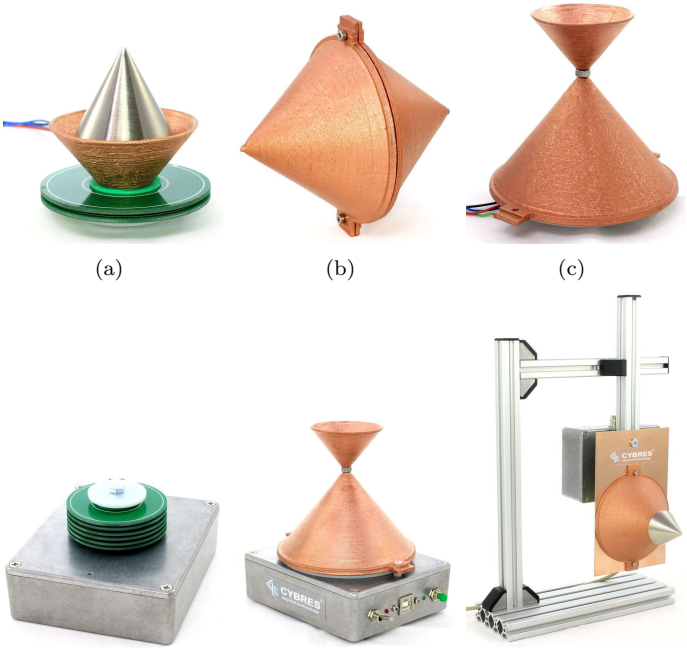

(a) (b) (c) (d) (e) (f)

Fig. 5. **(a)** An open circular Poynting vector (CPV) emitter, mounted on a small cone; **(b,c)** Emitter from (a), mounted inside a hollow copper cone; **(d)** Symmetrical structural element used in LAG; **(e,f)** CPV emitter with an increased number of circular dipoles, mounted on the EHM-C module housing; **(d)** Mounting the CPV emitter and the EHM-C control module on the holder

The emitter is mounted inside a large hollow cone (in the SAG manner), as shown in Fig. 5 (b,c). The outer cone also serves to protect the CPV emitter and to shield from EM fields. On a large cone, either a small cone for the PTT effect or a metal tip can be installed. Since modular structures are offered as a kit, it is even possible to create symmetrical emitters, see Fig. 5(b), known in LAG. The CPV emitter is mounted on a small cone, see Fig. 5(a) and can be used as a stand-alone device.

The electronics module, which generates signals for the emitter, is shown in Fig. 6(a), its structure is shown in Fig. 6(b). It is a microprocessor system with two cascade circuits for increasing the voltage up to 1200V, a current control circuit (up to 100 A in the pulse) and a modulation system for all voltages.

The company has been manufacturing EHM-C modules for several years, there are several modifications with various enclosures and 5V, 12V and 24V power systems. The configuration of voltages and control approaches is set by the user through the client program on the PC. In experiments described below, about 1000V of DC voltage was supplied to the CPV capacitor and about 200 mA of current at 5 (or 12) volts to the CPV coils.

As already mentioned, the development pursues the principle of modularity, therefore all components are offered separately as several sets. For example, the CPV

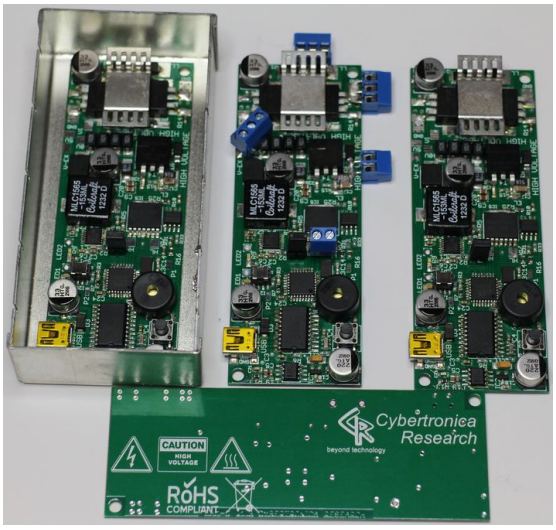

(a)

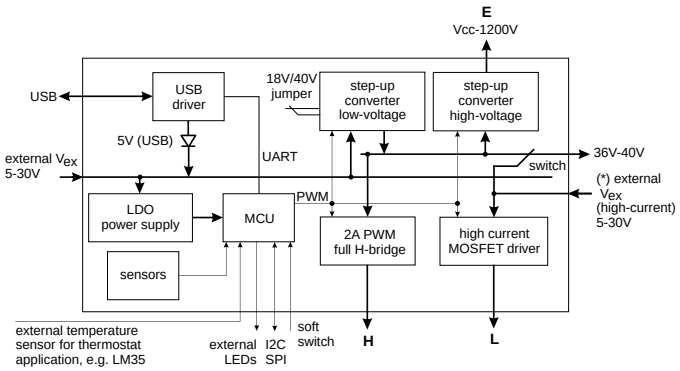

(b)

Fig. 6. **(a)** The EHM-C control module; **(b)** The structure of the EHM-C control module.

emitter can be mounted on the front part of a holder, and the EHM-C module at the rear, see Fig. 5(f). In a standard version, the CPV emitter is mounted on a solid aluminium housing with the EHM-C module that has an optional 5V power supply (from USB or 220V/110V) or 12V (from 220V/110V), see Fig. 5(e). The electronics allows reading the files generated by 'electronic modulators of PTT effect' and to modulate the E- or H-field components by signals from these files.

III. Performed tests with the generator

A. Control measurements

The electrochemical impedance spectroscopy (EIS) devices with differential impedance spectroscopy are used as sensors in these measurements [26], [27], [28]. Measuring effects of EM generators has some difficulties primarily due to temperature changes caused by the heating of coils and high-voltage electronics. Since the electrochemical sensors (outside the thermostat) react also to temperature changes, it is necessary to 'untie' the temperature and non-temperature factors. In general, the relationship between temperature and electrochemical measurements (e.g. electrical conductivity) is nonlinear [29]. Since the degree of nonlinearity is relatively small in the range 0-30° C, a linear approximating equation is used [30]:

$$EC_t = EC_{25}[1 + a(t - 25)], \tag{2}$$

where EC_t is the electrical conductivity at temperature t, EC_{25} is the electrical conductivity at 25°C, and a is the temperature compensation coefficient. In the work [31] various values of a in the range of 0.0191-0.025 are considered. For small temperature changes e.g. $\Delta t < 1$°C, we can assume that EC_t follows temperature with a certain coefficient. Large nonlinear variations of EC_t are introduced by non-temperature factors.

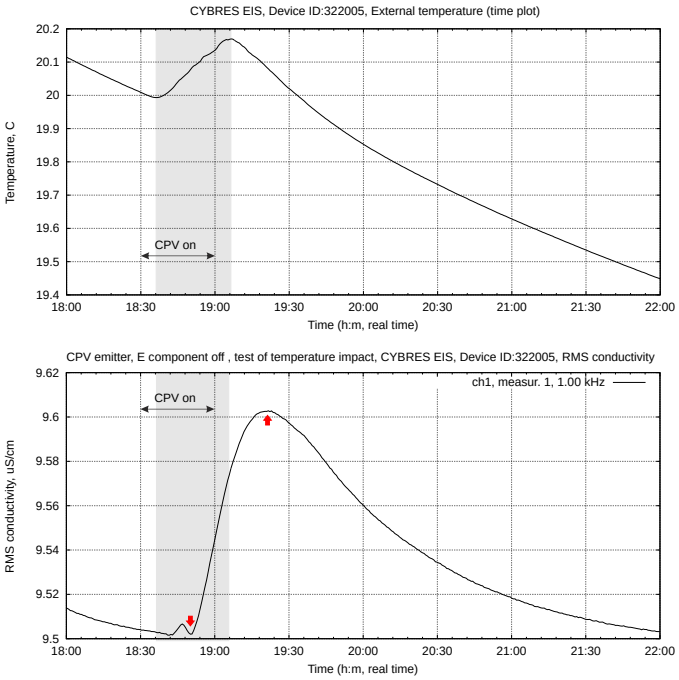

Fig. 7. EIS measurement of temperature dependence (2). The E-field is disabled, the Poynting vector is not generated, the temperature change occurs only due to heating of the coils. Time interval between inflection points of temperature and EIS curves (when turning the coil on and off) is about 7 minutes.

To confirm this statement, the EIS measurement was performed when the high-voltage part was switched off. The 5V voltage applied to the coils caused heating of the CPV emitter without generating the Poynting vector. For these tests, the electronic EHM-C module was disconnected from the emitter and moved out of the closed experimental chamber, so the temperature changes occurred only due to the heating of the emitter. To reduce heat production, the current was reduced to 2/3 of the maximum value, in addition the modulation with 50% meander applied, i.e. all tests passed at 1/3 of maximal power. The temperature sensor and the measuring container with water were mounted on the top of the large cone, see Fig. 5(c). The result of this EIS measurement is shown in Fig. 7. The EIS dynamics without the Poynting vector follows closely the temperature trend, as described by the equation (2). The time interval between inflection

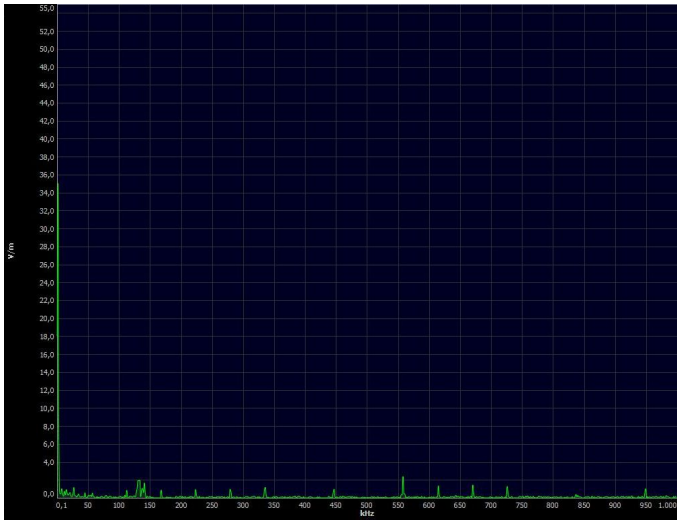

(a)

(b)

Fig. 8. Spectrograms **(a)** of alternating electric and **(b)** alternating magnetic fields at the distance 10mm from the grounded copper cone, the CPV emitter with the EHM-C generator is running. The measurement was carried out by the Spectran 5010 low-frequency spectrometer.

points of temperature and EIS curves is similar when the coil is turned on and off.

The second issue required to consider at such measurements is the electromagnetic shielding of both the control electronics modules and the emitters. To do this, all components of the generator are in metal housings, the copper cone of CPV emitter was grounded to a common ground wire. EM emission was measured with the Spectran 5010 device in the range from 100Hz to 1MHz, the spectrograms are shown in Fig. 8, the device was located at a distance of 10 mm. from the cone. The intensity of alternating electric field does not exceed 30V/m in the low-frequency part and not more than 4V/m at frequencies up to 1MHz. The intensity of alternating magnetic field does not exceed 100 nT in the low-frequency region and 10 nT at frequencies up to 1 MHz. These values are extremely low for rooms

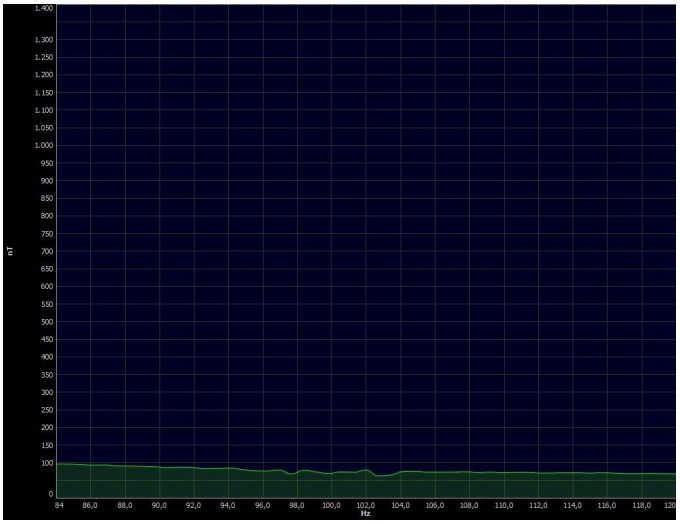

Fig. 9. Measurement of the alternating magnetic field when the H-field of the CPV emitter is set to the frequency of 100 Hz.

and do not change when the generator is turned on or off. For additional tests, the magnetic part of the CPV emitter was excited at the frequency of 100Hz and the H-field was measured in the range 84-120 Hz, see Fig. 9. This modulating frequency is not detected by Spectran 5010 near the emitter. Thus, these measurements allow us to conclude that the shielding of both the CPV emitter and the electronic module is sufficient.

B. Measuring the emission effects

For measurements one EIS sensor was mounted on the top of the cone, the second one was installed on the side (near the cone so that sensor touches it). This arrangement allows estimating the contributions of axial and radial components of the emission. The temperature sensor was installed at the top and at the side locations. Figure 10(a) shows the case when the EIS and temperature sensors are mounted in the top position, it corresponds to the experiment shown in Fig. 7, when the E-field is turned on and the Poynting vector is generated.

The generator was operated for 20 minutes, the temperature change was about 0.15° C, which is similar to the previous temperature test. However, the inflection points are positioned in this case differently, the starting point is closer to the temperature inflection, and the final point is shifted by 45 minutes after the temperature inflection (the 7 min. time interval between both points in the temperature test was almost equal to each other). These data point to other factors, beside temperature, that influence the EIS dynamics. We note once again that the conditions of both experiments are identical, the EM factor is eliminated by EM shielding, all experiments are carried out without light (full darkness). We also observe a higher intensity of the reaction. The EIS change in Fig. 7 was about 0.1 $\mu S/cm$, the EIS change in Fig. 10(a) is 0.16 $\mu S/cm$, i.e. almost 60% more intensive.

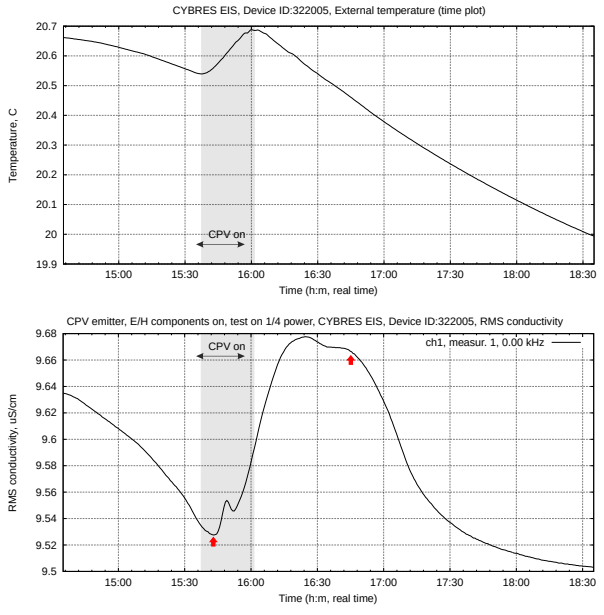

(a)

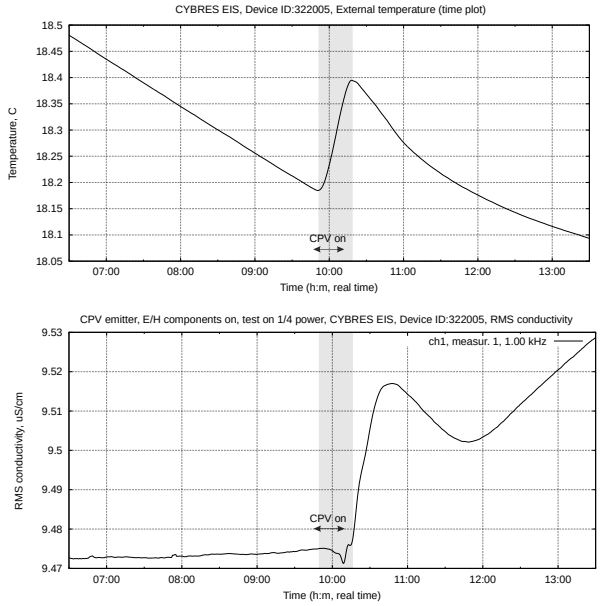

(b)

Fig. 10. **(a)** EIS measurement at the top of the cone, E/H fields are on, the Poynting vector is generated. Time interval between the first inflection points of temperature and EIS curves is about 3 minutes, the second inflection points – about 45 minutes; **(b)** EIS measurement of the exposed fluid from the previous experiment performed on the next day. The 'paradoxical phase' is observed, which violates the temperature dependence expressed by the equation (2).

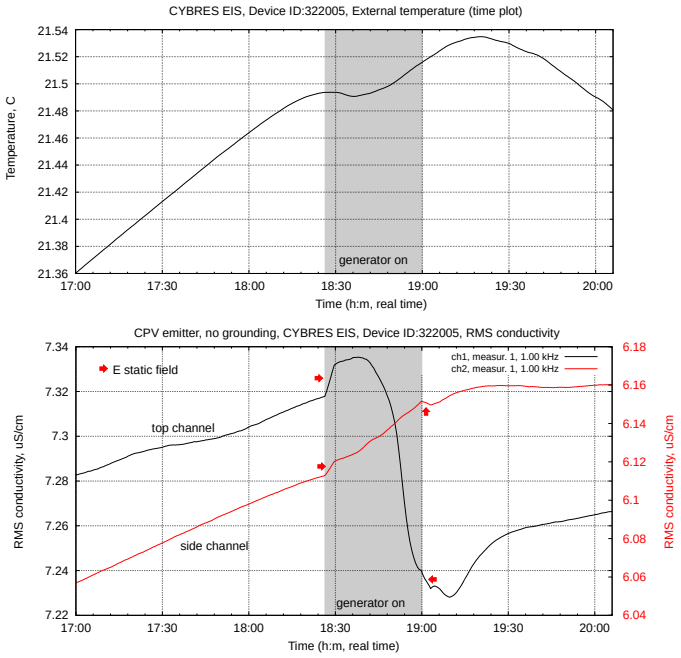

Fig. 11. Tests for axial and radial effects, channel 1 is installed on the top of the cone, channel 2 on the base, the containers touch the metal cone, the grounding of copper cone is removed.

It is known that the exposed fluids behave electrochemically different than non-exposed fluids. For example, the performed tests [32] demonstrated the appearance of a 'paradoxical phase' that violates one of the fundamental electrochemical dependencies – the temperature dependency expressed by the equation (2). For tests of this phenomenon, the water used in the previous experiment was left for one night in measurement chamber, and the second EIS measurement was performed on the next day. The result of this second measurement is shown in Fig. 10(b), where the 'paradoxical phase' is clearly visible – in response to decreasing temperature, the amplitude of the EIS dynamics increases.

For further tests of the axial direction, the CPV emitter was taken out of a cone and mounted on the holder. The emitter was placed on a plastic part to decouple it from the grounded housing of the control module. The idea is that grounding of the cone can affect its efficiency. To prevent EM impact, a grounded sheet 0.3 mm of steel with a size of 300x200 mm is installed between EIS sensors and the CPV emitter. Despite this shielding is not not full (i.e. it does not create a Faraday cage), the goal of this test was to demonstrate changes that can last for hours after the generator was turned off. Such long-term post-experimental changes are uncharacteristic for EM emissions.

Results of these EIS measurements are shown in Fig. 12. The response of EIS sensors starts with a delay of about 2.5 minutes (the distance between the radiator and the sensors is 20 cm), and there is no change of temperature trend on the sensor side. When the generator is turned off, the effect slowly disappears: with a 30-minute operation of the generator, the post-experimental EIS dynamics (disappearance of changes) takes about 180 minutes. The spikes in the graph after exposure indicate the effect of proton tunneling in water, responsible for the anomalous conductivity. Thus, both the duration and the characteristics of the EIS changes after turning off the generator are uncharacteristic for EM emissions.

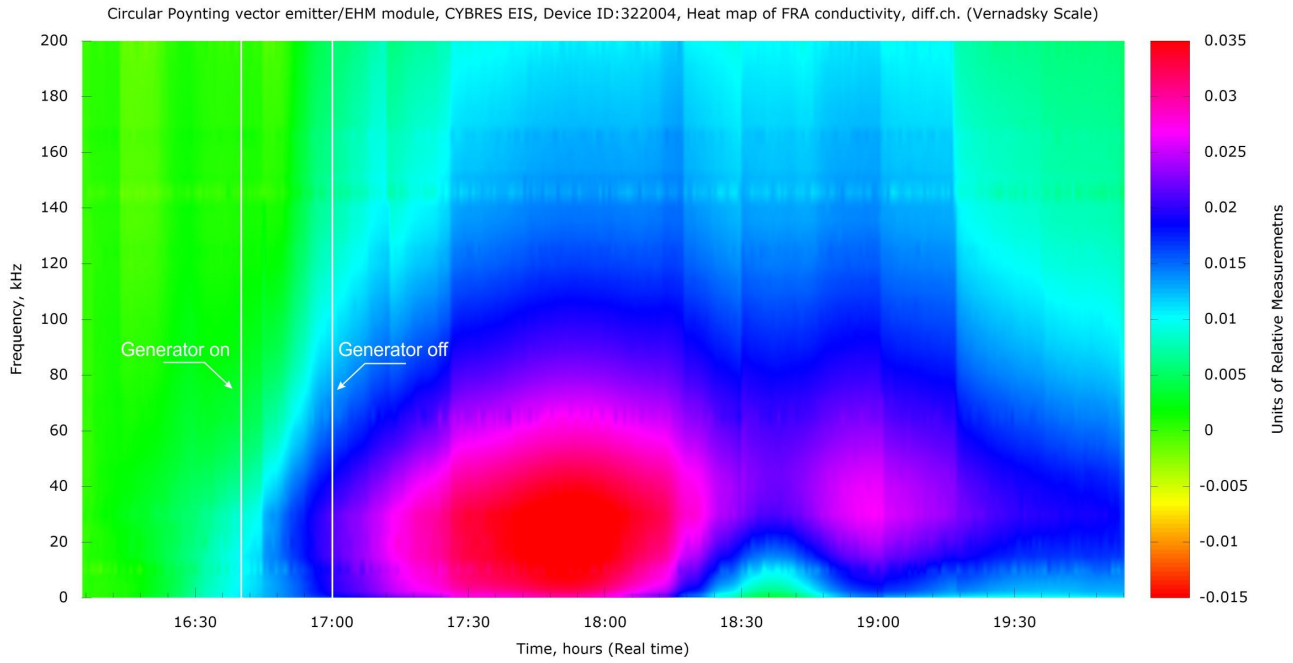

Fig. 12. EIS dynamics, the turn-on time of the generator is shown by lines, the appearance of (quantum) proton tunnelling effect in the form of jumps in the graph is observed, the operating time of the generator is 30 minutes, the post-EIS dynamics (disappearance of changes) is about 180 minutes.

C. Tests of axial and radial effects

As mentioned above, the state-of-the-art effects published in relation to the Poynting vector (see e.g. [33]) were taken into account in the design of CPV emitter. The design of LAG, see Fig. 2(b), possesses different conic elements connected by metal wires. Authors of LAG argue that the metallic cones should have two effects: firstly, they serve as concentrators (by analogy with high-frequency EM emission that is sensitive to geometry of functional elements), and secondly, they have a shielding role for EM emission from generators. It is expected that the axial (on the top of a cone) and radial positions of samples will result in different effects.

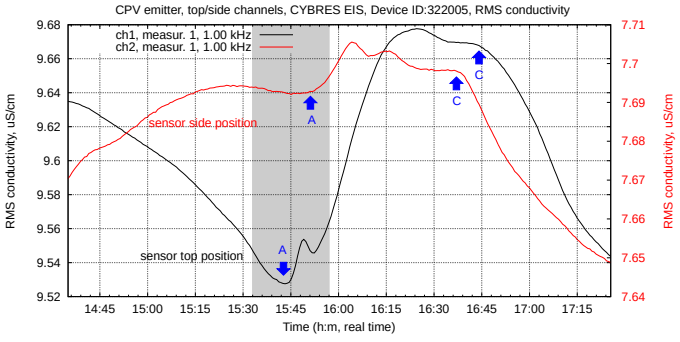

Fig. 13. Tests for axial and radial effects, comparison of the EIS channels mounted on the top of the cone and at the base, see the previous experiment, shown in Fig. 10(a).

To test this hypothesis, the previous setup was used – one EIS container at the top of the cone, the second on the side on the base, both plastic containers with water touch the metal cone. The cone grounding is removed, the temperature sensor is mounted on the side container. The result of the EIS measurement is shown in Fig. 11. An obvious effect is the potential jumps when the generator is turned on and off, which is explained by the appearance of a static E-field. Based on the example of channel 2, we can conclude it affects the EIS dynamics, but its contribution is small even in comparison with the temperature effect. The channel 2 located in the radial direction follows a temperature trend, whose variation is smaller since the temperature sensor does not touch the metal cone. There is a faster reaction of the EIS sensors compared to previous experiments with grounded cones (however, here the question arises of the contribution of the static E-field). Comparing the axial and radial arrangements, we can see that changes in the axial arrangement (channel 1) at the top position are much more intense. Similar data were obtained in other experiments, for example Fig. 13 shows both channels of the previous experiment performed with another set of electrodes. The EIS channel at the top position of the cone has a larger amplitude and a faster response, which indicates a predominance of the axial direction in the effect of CPV.

D. Measuring effects of liquids exposure

The well-known applications of SAG/LAG are related to the PTT effect, when exposed liquids and solid substances during phase-transition stage demonstrated different physical and chemical properties. As an example, the Fig. 2(c) demonstrates the SAG-based setup, used for exposure of solid materials in experiments around 2000 in

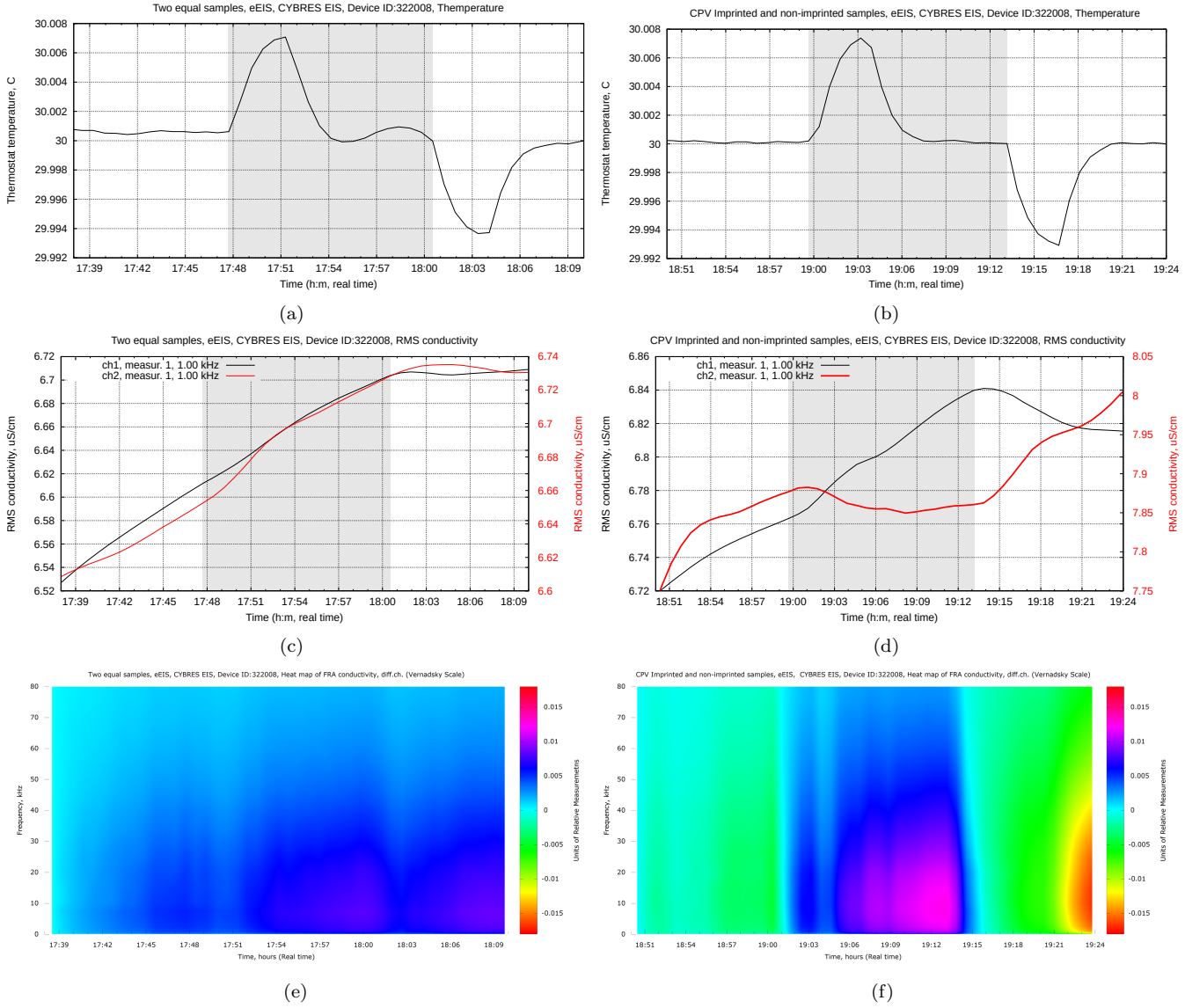

Fig. 14. Express analysis of two pairs of fluids: **(a,c,e)** analysis of two identical not-exposed-by-emission fluids in the control pair; **(b,d,f)** analysis of two liquids in the experimental pair, one of which was exposed for 30 minutes at the top position of the CPV emitter. Degassing of fluids (repeated removal of electrodes from containers) was not performed for both attempts.

South Korea, see also other examples of this approach in metallurgy [24].

The works of V.A.Sokolova [34] were especially intensive in this respect, we already repeated some experiments of this group [28]. In these experiments, two identical samples were prepared and compared by the impedance spectroscopy, then one of them was irradiated by a generator without PTT, and then these two samples were compared again. Figure 14 shows the results of a similar experiment, carried out by the modern method of EIS express analysis. Four samples (two pairs) of 10 ml of distilled water are prepared. One pair represents a control pair for the differential measurement, one liquid in the second pair was treated for 30 minutes at the top position of the CPV emitter. That pair represents an experimental pair for the differential measurement. Both pairs were prepared and analyzed in a similar way in the thermostat, the same time was given for temperature equalization, moreover, all samples were analyzed for a short time one after the other – first the control pair, then the experimental pair. As shown by Fig. 14(c), the behavior of the EIS curves in the control pair is very similar, their differential spectra in Fig. 14(e) are rather homogeneous. The behaviour of the experimental pair in Fig. 14(d) differs substantially from each other, their differential spectra in Fig. 14(f) shows a characteristic pattern of differences. Thus, we observe a similar effect with the results obtained by the Sokolova's group – a non-chemical treatment for a short time substantially changes the electrochemical dynamics of the exposed liquid.

For further tests with exposed liquids by PTT effect, we used the generator shown in Fig. 5(e) powered by 12V (from 110V/220V AC-DC converter) with one circular dipole element. The maximal current through coils was

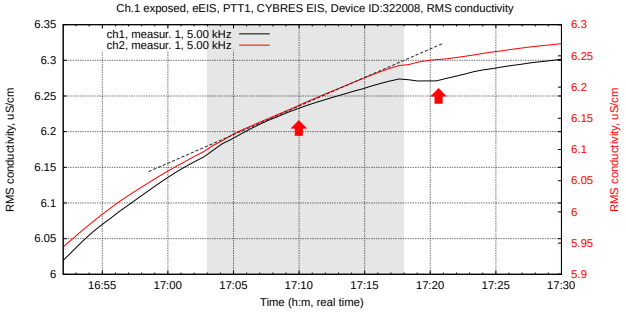

(a)

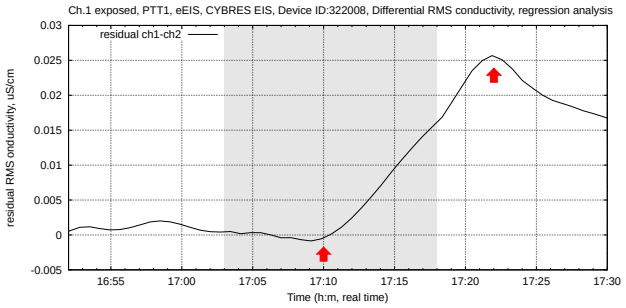

(b)

Fig. 15. Exposure of liquids, PTT1, the sample N5, the channel 1 is the exposed (experimental) channel, the channel 2 is the control channel; **(a)** two channels representation; **(b)** the regression analysis of differential channel, see description in text. Degassing of fluids was performed.

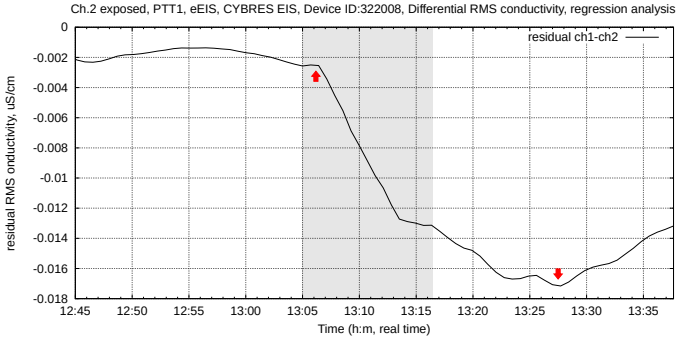

Fig. 16. Example of repeated attempts with changed channels, PTT1: the channel 2 is the exposed channel, the channel 1 is the control channel. Shown is the regression analysis of differential channel, see Fig. 15(b). The exposure time is doubled, the degassing of fluids was performed.

increased up to 0.4A with about 1000V on the capacitor. The regression analysis was employed for detecting differences between exposed and unexposed fluids, other parameters are similar to the previous tests. For the PTT with $C_{12}H_{22}O_{11}$ (denoted as PTT1), 12g. of the substance was placed in the small upper cone. The EIS container was placed on the top without touching the walls of copper cone. The experimental parameters are similar to the previous attempts: exposition time 20 minutes, all samples are exposed one after another within a short time interval.

In the first day we performed 5 attempts, the exposure-measuring-cycle of one sample took about 1 hour. The first noted issue is the variation of intensity from 1st to 5th sample – usually the first exposed sample demonstrated the strongest results, like shown in Fig. 14. Secondly, exchanging control and experimental channels of the EIS spectrometer in following after each other measurements led to unstable EIS dynamics of both channels. The best conditions are long resting time between expositions, using the same control/experiment channels within one experimental series and different plastic containers in each attempt. In Fig. 15 we demonstrate the EIS measurement of the last 5th sample, it is well visible that the exposed channel 1 behaves differently that the unexposed channel 2. In fact all inflection points of the differential curve obtained by regression analysis are caused by the exposed channel 1.

To test the results on technological or measurement artefacts, we repeated these attempts on the next day, but changed the impacted channel – now the channel 2 was the exposed channel, and the channel 1 is the control channel.

The regression analysis of differential channel is shown in Fig. 16. We observe here the inverse type of dynamics of the Fig. 15(b) pointing to absence of technological artefacts in the measurements. There are also some variations of intensity and timing of inflection points that can be attributed to slightly different conditions of these repeated experiments.

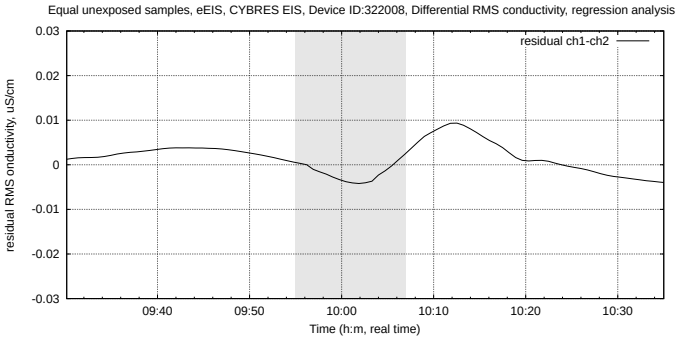

Fig. 17. Control attempt with unexposed fluids, the degassing of fluids was performed.

Several control experiments with unexposed fluids and degassing procedure was performed between the PTT1 and the next attempts with PTT2, one of them is shown in Fig. 17. In fact we observe a similar behaviour as shown in Fig. 14, however with smaller amplitude of variation. The final series of experiments were the attempts with $NaCl$ (denoted as PTT2), all parameters are similar to the PTT1 experiments. One experimental result is shown in Fig. 18, we observe the residual EIS dynamics that differs from PTT1 and control measurements that can be accounted to PTT2 effect (among other factors) in the exposed channel 1. We performed two measurements within 2 hours, which demonstrated a similar dynamics (with linear transformation required due to linear shift of differential curve) – this points to a reproducibility of results. 3D Spectrograms of data from Fig. 18 are shown in Fig. 19, which demonstrate interesting symmetrical activation patterns.

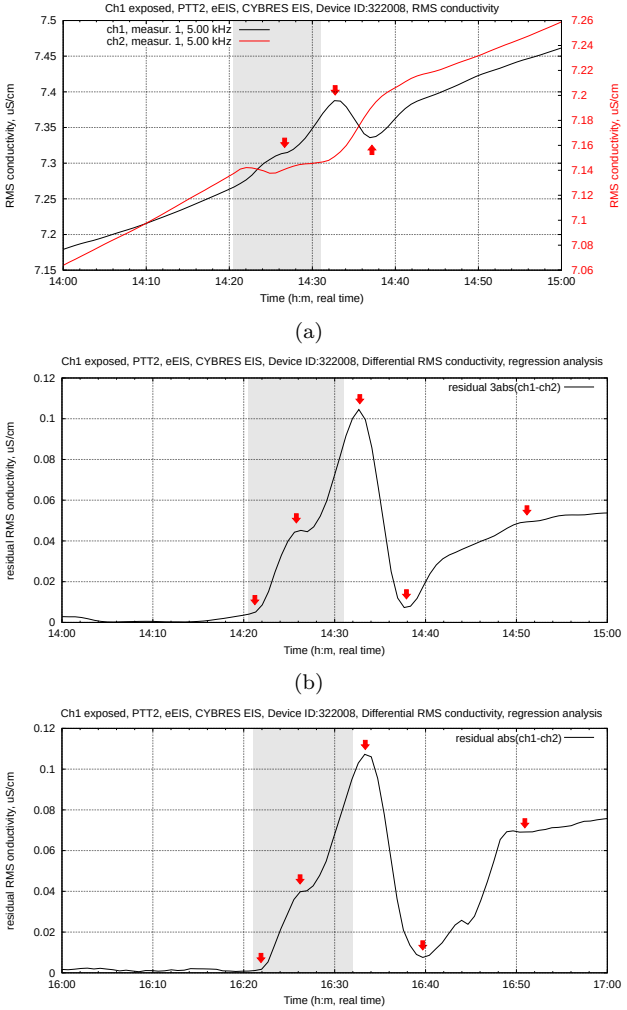

Fig. 18. Exposure of liquids, PTT2, the channel 1 is the exposed (experimental) channel, the channel 2 is the control channel, the degassing of fluids was performed. **(a)** Two channels representation, characteristic changes are in the exposed channel 1; **(c,d)** Two measurements with linear transformation performed within 120 minutes.

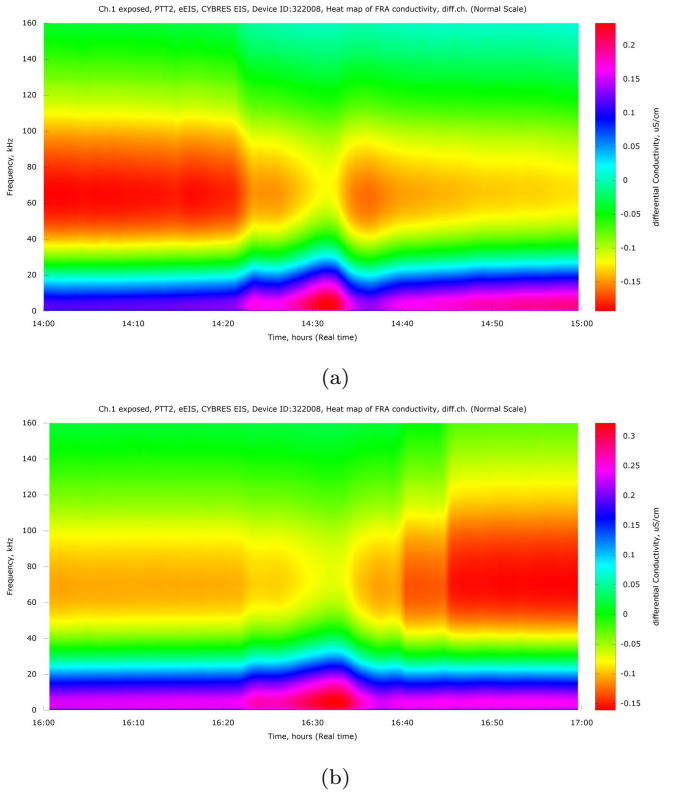

Fig. 19. 3D Spectrograms of two attempts from Fig. 18.

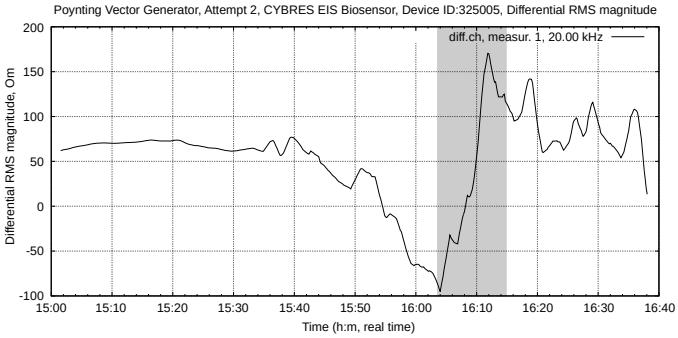

Fig. 20. **(a)** Exposing experimental samples of water with sugar (for biological tests) on the generator; **(b)** Identification of different phases of fermentation based on the dynamics of differential RMS impedance.

E. Measuring biological effects

For testing biological effects, the CYBRES Biosensor based on the fermentation activity of yeast *Saccharomyces cerevisiae* was used. The experimental samples of water with sugar are exposed on the generator for 60 minutes. After this, the experimental and control samples were rested in the water bath for 10 min to equalize the temperature and then the yeast solution were added to the containers.

For analyzing the results, we used the phase characteristics – specific stages of fermentation start earlier (or later) depending on stimulating (or inhibiting) effect of exposure. For identification of a phase the differential RMS impedance is utilized, see Fig. 20(a), different stages of fermentation are characterized by an essential change (e.g. different slope) of EIS dynamics, see for more detail [35]. As required by the double differential measurement approach, we performed two measurements: first, the channel 1 was the experimental channel, in the second attempt the channel 2 was experimental one. This approach enables identification of measurement artefacts and errors.

Figures 21(a) and 21(b) show the EIS dynamics of both control and experimental channels for these two attempts, the identified fermentation stages are shown by a grey bar. The resulting phase difference between control and experimental channels for both attempts are shown in Fig. 21(c). We observe more earlier start of fermentation in the exposed channel in both attempts, this points to a stimulating effect on activities of microorganisms by the generator.

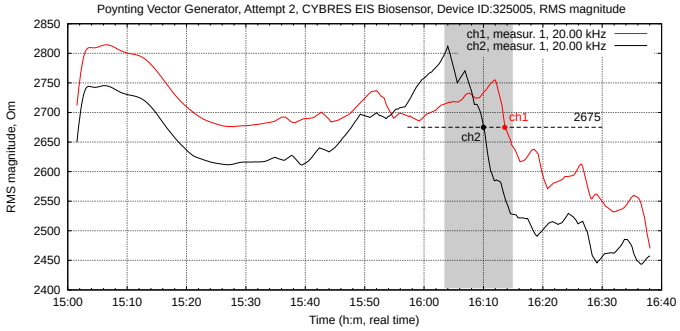

(a)

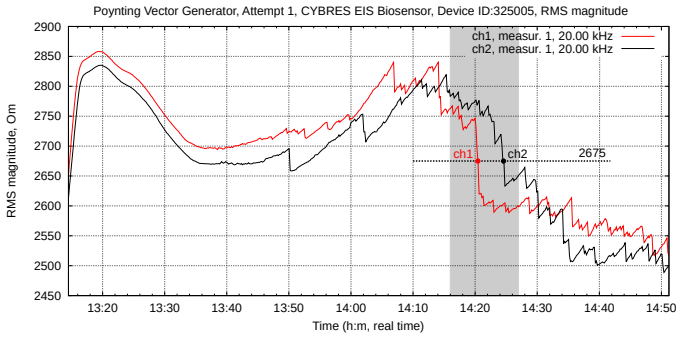

(b)

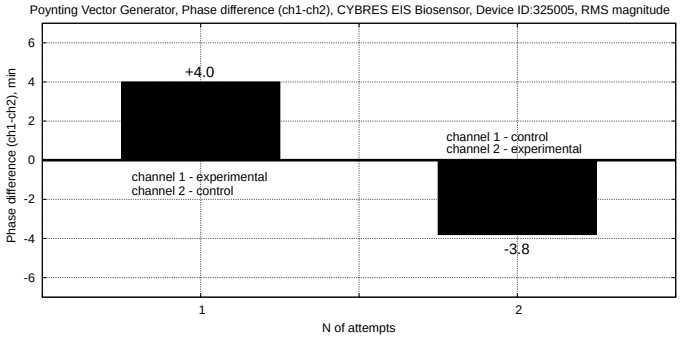

(c)

Fig. 21. Biological tests with CYBRES Biosensor based on the fermentation activity of yeast *Saccharomyces cerevisiae*. Two double differential attempts with inverse channels (the attempt 1: the channel 1 is the experimental channel; the attempt 2: the channel 2 is the experimental channel) are shown. **(a,b)** EIS dynamics of control and experimental channels for attempts 1 and 2, the identified fermentation stages are shown by a grey bar; **(c)** the resulting phase difference between control and experimental channels for both attempt, the exposed channel in both attempts demonstrate a stimulating effect on activities of microorganisms.

IV. Conclusion

Based on experimental results, we can conclude with sufficient confidence that the CPV emitter with one circular dipole demonstrates effects that are similar to the previously investigated effects of the optical LED emitter [36], [25]. There are observed effects of delayed EIS dynamics, mismatch with temperature curves, the appearance of 'paradoxical phases', accumulation of emission after the generator is turned off. Comparing the axial and radial directions, we note more intense reaction of the EIS sensors in the axial direction at the top of the cone. This is unusual, since both containers are at the distance of 10 cm from each other and should show a similar dynamics, when do not take into account the generated emission. Express analysis of the irradiated sample gives results similar to the V.A.Sokolova's group, which were obtained for the Deev's and Akimov's generators. Considering results of liquids exposure, described in Sec. III-D, we note primarily the experimental confirmation of electrochemical differences between exposed and unexposed liquids. Also, a stimulating biological effect on microorganisms is registered in the position at the 'top of the cone'. After numerous experiments, we decided to leave the external elements of the generator without grounding - on the one hand this increases its efficiency, but on the other hand it is necessary to keep in mind the arising electrostatic charge.

The structure of the CPV emitter and the EHM-C module follows the concept of the 'small Akimov's generator' and implies the same applications. However, we choose more open approach for devices and publications, when the modular generation technology, different encountered effects and detecting/sensing devices are provided to users. We point to safety methods when using these technologies, in particular a strong recommendation to allocate a separate room for these works without biological organisms, and to limit the intensity of generated emissions to a minimal level.

References

[1] S. Kernbach, A. Kernbach, A. Rusanov, and I. Volkov. Analysis of the ochatrin's detector and the smal akimov's generator. *IJUS*, 9(3):70–89, 2015.

[2] A.E.Akimov, B.I.Petrovcky, and V.J.Trasenko. *Structure and construction of torsion generators, pre-pring N52 (rus)*. M., MNTC VENT, 1995.

[3] S. Kernbach. Unconventional research in USSR and Russia: short overview. *arXiv 1312.1148*, 2013.

[4] V.I.Lunev. *Experimental research in the field of spin-torsion interactions (rus)*. Tomsk, 1995.

[5] O.B.Bron. *Electromagnetic fields as a kind of matter (rus)*. M., State Energy Publishing House, 1962.

[6] V.N. Anosov and E.M. Truchan. New approach to impact of weak magnetic fields on living objects (rus). *Doklady Akedemii Nauk: biochemistry, biophysics and molecular biology*, (392):1–5, 2003.

[7] E.M Trukhan. Impact of weak electro-magnetic fields on biological activity of water phase (rus). *Computer Research and Modeling*, 1(1):101–108, 2009.

[8] Ivan Rampl, Vladimír Boudný, Milan Cíž, Antonín Lojek, and Pavel Hyršl. Pulse vector magnetic potential and its influence on live cells. In *Proceedings of the 2009 International Conference on eHealth, Telemedicine, and Social Medicine*, ETELEMED '09, pages 99–107, Washington, DC, USA, 2009. IEEE Computer Society.

[9] Y. Aharonov and D. Bohm. Significance of Electromagnetic Potentials in the Quantum Theory. *Physical Review Online Archive (Prola)*, 115(3):485–491, 1959.

[10] K.A. Trukhanov. Possible role of the aharonov-bohm effect in the biological action of a magnetic field. *Kosm Biol Aviakosm Med.*, 12(3):82–3, 2078.

[11] V. Rubaev and L. Fedichkin. The Aharonov Bohm effect as a material phenomenon. *arXiv, 10.48550/ARXIV.2109.12438*, 2021.

[12] Vlatko Vedral. Quantifying entanglement in macroscopic systems. *Nature*, 453(7198):1004–1007, 2008.

[13] J. Sperling and I. A. Walmsley. Entanglement in macroscopic systems. *Phys. Rev. A*, 95:062116, Jun 2017.

[14] Rodrigo A Thomas, Michał Parniak, Christoffer Østfeldt, Christoffer B Møller, Christian Bærentsen, Yeghishe Tsaturyan, Albert Schliesser, Jürgen Appel, Emil Zeuthen, and Eugene S Polzik. Entanglement between distant macroscopic mechanical and spin systems. *Nature Physics*, 17(2):228–233, 2021.

[15] Ying Li, Ya-Feng Jiao, Jing-Xue Liu, Adam Miranowicz, Yun-Lan Zuo, Le-Man Kuang, and Hui Jing. Vector optomechanical entanglement. *Nanophotonics*, 11(1):67–77, 2022.

[16] C. Marletto, D. M. Coles, T. Farrow, and V. Vedral. Entanglement between living bacteria and quantized light witnessed by rabi splitting. *Journal of Physics Communications*, 2(10):101001, 2018.

[17] K. S. Lee, Y. P. Tan, L. H. Nguyen, R. P. Budoyo, K. H. Park, C. Hufnagel, Y. S. Yap, N. Mobjerg, V. Vedral, T. Paterek, and R. Dumke. Entanglement between superconducting qubits and a tardigrade. *arXiv 2112.07978*, 2021.

[18] Olga Bolshakova. *The 'Maslobrod Effect' (rus)*. Russian Word, N13 (641) 6.04.2018, 2018.

[19] A.Y. Smirnov. Long-range nonlocal interactions in 'teleportation' of information (rus). *Proc. of II int. conf. 'Torsion fields and information interactions'*, pages 119–149, 2010.

[20] S. Kernbach, V.T. Shkatov, and V. Zamsha. Report on experiment with super-long range signal transmission by using a digital representation of planet Mars (rus). *International Journal of Unconventional Science*, 2(1):61–75, 2013.

[21] OPPGT Document No. 1220. *Evaluation of Non-Chemical Treatment Technologies for Cooling Towers at Select California Facilities*. California Department of Toxic Substances Control Office of Pollution Prevention and Green Technology, 2009.

[22] F. Alimi, M.M. Tlili, M. Ben Amor, G. Maurin, and C. Gabrielli. Effect of magnetic water treatment on calcium carbonate precipitation: Influence of the pipe material. *Chemical Engineering and Processing: Process Intensification*, 48(8):1327 – 1332, 2009.

[23] K.K Jyoti and A.B Pandit. Water disinfection by acoustic and hydrodynamic cavitation. *Biochemical Engineering Journal*, 7(3):201 – 212, 2001.

[24] A.V.Kluev, S.A.Kurapov, V.F.Panov, V.V.Strelkov, N.A.Kokarev, and A.E.Boajrishnikov. Structure and mechanical properties of metals after processing in a nonstationary electromagnetic field (rus). *Metallurgy, thermal processing of metals*, (7 (649)):3–9, 2009.

[25] Serge Kernbach. Replication attempt: Measuring water conductivity with polarized electrodes. *Journal of Scientific Exploration*, 27(1):69–105, 2013.

[26] S. Kernbach, I. Kuksin, O. Kernbach, and A. Kernbach. The vernadsky scale – on metrology of EIS in time-frequency domain. *IJUS*, 143–150(5):62–87, 2017.

[27] S. Kernbach, I. Kuksin, and O. Kernbach. Analysis of ultraweak interactions by electrochemical impedance spectroscopy (rus). *IJUS*, 11(4):6–22, 2016.

[28] S. Kernbach, I. Kuksin, and O. Kernbach. On accurate differential measurements with electrochemical impedance spectroscopy. *WATER*, 8:136–155, 2017.

[29] F.J. Millero. *The Physical Chemistry of Natural Waters*. Wiley-Interscience, New York, 2001.

[30] John A. Sorensen and Gary E. Glass. Ion and temperature dependence of electrical conductance for natural waters. *Analytical Chemistry*, 59(13):1594–1597, 1987.

[31] Masaki Hayashi. Temperature-electrical conductivity relation of water for environmental monitoring and geophysical data inversion. *Environmental Monitoring and Assessment*, 96(1):119–128, Aug 2004.

[32] S. Kernbach. On symbols and mems. Part 2. *IJUS*, 19-20(6):120–148, 2018.

[33] S. Kernbach. *Supernatural. Scientifically proven facts (rus)*. ISBN: 978-5-906789-00-6, Algorithm. Moscow, 2015.

[34] V.A. Sokolova. *First experimental confirmation of torsion fields and their usage in agriculture (rus)*. Moscow, 2002.

[35] Serge Kernbach, Olga Kernbach, Igor Kuksin, Andreas Kernbach, Yury Nepomnyashchiy, Timo Dochow, and Andrew Bobrov. The biosensor based on electrochemical dynamics of fermentation in yeast *Saccharomyces Cerevisiae*. *Environmental Research (preprint 10.48550/ARXIV.2202.07795)*, 2022.

[36] S. Kernbach. Exploration of high-penetrating capability of LED and laser emission. Parts 1 and 2 (rus). *Nano- and microsystem's technics*, 6,7:38–46,28–38, 2013.